Journal of Magnetism and Magnetic Materials 321 (2009) 3256–3261

Contents lists available at ScienceDirect

Journal of Magnetism and Magnetic Materials

journal homepage: www.elsevier.com/locate/jmmm

Frustrated magnetic structure of TmAgGe

S. Baran [a,*], D. Kaczorowski [b], A. Arulraj [c], B. Penc [a], A. Szytuła [a]

[a] M. Smoluchowski Institute of Physics, Jagiellonian University, Reymonta 4, PL-30 059 Kraków, Poland
[b] Institute of Low Temperature and Structure Research, Polish Academy of Sciences, P. O. Box 1410, PL-50 950 Wrocław, Poland
[c] Helmholtz-Zentrum Berlin, Glienicker Str. 100, D-14 109 Berlin, Germany

ARTICLE INFO

Article history:
Received 11 May 2009
Available online 6 June 2009

PACS:
65.40.−b
75.25.+z
75.30.Cr
75.50.Ee

Keywords:
Rare earth intermetallics
Frustrated antiferromagnet
AF magnons
Neutron scattering

ABSTRACT

Physical properties of the compound TmAgGe have been investigated by means of magnetometric, transport, calorimetric as well as neutron diffraction measurements. The compound crystallizes in the hexagonal ZrNiAl-type crystal structure. The reported results indicate that the sample exhibits an antiferromagnetic ordering below $T_N = 4.2$ K. The low temperature behavior of the magnetic susceptibility and the specific heat is in good agreement with the spin-wave theory with linear dispersion relation. In addition, the magnetic structure of TmAgGe was determined by means of neutron diffraction measurements. The Tm moments are equal to 6.44(10) μ_B at 1.5 K and form a non-collinear magnetic structure within the basal plane. To describe this structure three different propagation vectors: $\vec{k} = [\frac{1}{2}, 0, 0]$, $\vec{k}' = [-\frac{1}{2}, \frac{1}{2}, 0]$ and $\vec{k}'' = [0, \frac{1}{2}, 0]$ are required. Such a spin arrangement is analyzed on the basis of group theory.

1. Introduction

The RAgGe (R = rare earth) ternary intermetallics crystallize in the hexagonal crystal structure of the ZrNiAl-type [1,2]. In this type of structure the rare earth ions occupy equivalent 3g positions with an orthorhombic point symmetry. The results of magnetic measurements, performed on polycrystalline and single-crystalline samples of these compounds, revealed in several of them antiferromagnetic ordering in the ground state and strong influence of the crystalline electric field (CEF) effect in both the ordered and paramagnetic regions [3–7]. In particular, TmAgGe was characterized as an antiferromagnet with the Néel temperature 4.2(1) K [5], easy-plane magnetic anisotropy and distinct metamagnetic features observed for magnetic field applied perpendicular to the *c*-axis [6].

In the present work the magnetic ordering in TmAgGe has been probed by neutron powder diffraction, and the physical properties of the compound have been investigated within wide temperature range by magnetization, electrical resistivity and heat capacity measurements.

2. Experimental details

Polycrystalline sample of TmAgGe was synthesized by arc melting high-purity elements (Tm: 3N; Ag: 4N; Ge: 5N) under titanium-gettered argon atmosphere. In order to ensure appropriate homogeneity the resulting ingot was turned over and remelted several times. Afterwards, the sample was annealed in an evacuated quartz ampoule at 600 °C for one week.

The product quality was examined by X-ray powder diffraction at room temperature on a Philips PW-3710 X'PERT diffractometer using CuK_α radiation. The results confirmed the hexagonal ZrNiAl-type crystal structure and indicated almost single-phase character of the prepared sample.

Magnetic measurements were performed within the 1.72–300 K temperature range and in external magnetic fields up to 5 T using a Quantum Design SQUID magnetometer. The electrical resistivity was measured over the temperature interval of 3.8–290 K employing a standard dc four-probe technique and a home-made setup. Heat capacity studies were carried out in the temperature range 0.3–300 K using a relaxation method implemented in a Quantum Design PPMS platform.

The neutron powder diffraction patterns were collected on the E6 diffractometer installed at the BERII reactor (Helmholtz–Zentrum Berlin) within the temperature range from 1.5 to 6.1 K. The incident neutron wavelength was 2.452 Å. The neutron diffraction data were analyzed using the Rietveld-type program FullProf [8].

3. Results and discussion

3.1. Crystal structure

The X-ray diffraction data, collected at room temperature, as well as the neutron diffraction data, obtained at 6.1 K

* Corresponding author. Tel.: +48 12 6635686; fax: +48 12 6337086.
E-mail address: stanislaw.baran@uj.edu.pl (S. Baran).

0304-8853/$ - see front matter © 2009 Elsevier B.V. All rights reserved.
doi:10.1016/j.jmmm.2009.05.064

(paramagnetic state), confirmed unambiguously the hexagonal ZrNiAl-type structure (space group $P\bar{6}2m$) of TmAgGe. In this unit cell the particular atoms occupy the following sites:

3 Tm atoms at 3(g) site $x_{Tm}, 0, \frac{1}{2}$ $0, x_{Tm}, \frac{1}{2}$ $\overline{x}_{Tm}, \overline{x}_{Tm}, \frac{1}{2}$

3 Ag atoms at 3(f) site $x_{Ag}, 0, 0$ $0, x_{Ag}, 0$ $\overline{x}_{Ag}, \overline{x}_{Ag}, 0$

2 Ge atoms at 2(c) site $\frac{1}{3}, \frac{2}{3}, 0$ $\frac{2}{3}, \frac{1}{3}, 0$

1 Ge atom at 1(b) site $0, 0, \frac{1}{2}$

The values of the lattice parameters and the free positional parameters x derived from the neutron diffraction pattern are listed in Table 1.

3.2. Magnetic behavior

The magnetic properties of TmAgGe are presented in Fig. 1. Above about 80 K, the inverse magnetic susceptibility exhibits a linear-in-T behavior. At lower temperatures some curvature of $\chi^{-1}(T)$ is seen, presumably due to CEF effect. Fitting the Curie–Weiss formula to the experimental data yielded the paramagnetic Curie temperature $\theta_p = 12.1(1)$ K and the effective magnetic moment $\mu_{eff} = 7.37(4)\ \mu_B$. The experimental value of μ_{eff} is close to the free Tm^{3+} ion value (7.56 μ_B). As shown in the upper inset in Fig. 1, the compound orders magnetically at 4.2 K and the observed anomaly is typical for antiferromagnets. Very similar result was reported for TmAgGe in Ref. [5]. The antiferromagnetic character of the magnetic ordering is corroborated by behavior of the isothermal magnetisation taken at 1.72 K as a function of magnetic field up to about 5 T. A clear metamagnetic transition is visible at $B = 0.3$ T (see the lower inset to Fig. 1). This value is in good agreement with the data found for single crystal (see in Ref. [6, Fig. 18]). The saturation magnetic moment in the field-induced ferromagnetic state at 1.72 K equals 3.9(3) μ_B, which is much smaller than the free Tm^{3+} ion value (7.0 μ_B) and should be related to the CEF electronic ground state of the compound.

Table 1
Refined structural parameters of TmAgGe together with residuals for profile and integrated intensities.

a (Å)	7.026(2)
c (Å)	4.143(2)
c/a	0.5897(4)
V (Å^3)	177.1(2)
x_{Tm}	0.576(2)
x_{Ag}	0.250(2)
χ^2	4.83
$R_{profile}$ (%)	2.62
R_{Bragg} (%)	5.95

The parameters were derived from neutron diffraction patterns collected at 6.1 K.

3.3. Electrical resistivity

The results of electrical transport measurements of TmAgGe are presented in Fig. 2. The compound exhibits metal-like electrical conductivity with a faint anomaly at low temperatures due to magnetic ordering at $T_N = 4.2$ K. The latter feature manifests itself as a sudden drop in the temperature derivative of the resistivity (see the lower inset in Fig. 2). Above the Neel temperature the resistivity goes through a broad local minimum around 15 K. In the region where the magnetic contribution to the electrical resistivity can be assumed to be nearly temperature independent (i.e. where the CEF effects do not play major role), the resistivity data can be described using the Bloch–Grüneisen–Mott (BGM) formula:

$$\rho(T) = (\rho_0 + \rho_\infty) + 4RT\left(\frac{T}{\Theta_D}\right)^4 \int_0^{\Theta_D/T} \frac{x^5\,dx}{(e^x - 1)(1 - e^{-x})} - KT^3 \qquad (1)$$

where the first term is a sum of the residual ρ_0 and spin-disorder ρ_∞ resistivities, whereas the electron-phonon scattering processes and the s–d interband scattering processes are described by the second and the third term, respectively. Fitting Eq. (1) to the experimental data in the range 125–290 K gives the following set of parameters: $(\rho_0 + \rho_\infty) = 253.7\ \mu\Omega\,cm$, $R = 1.086\ \ \mu\Omega\,cm/K$, $\Theta_D = 257.7$ K and $K = 2.19 \times 10^{-6}\ \mu\Omega\,cm/K^{-3}$. The parameter Θ_D is usually treated as a rough estimation of the Debye temperature, despite its value is somehow influenced by electronic correlations [9]. In the case of TmAgGe, however, the so-obtained Θ_D appears to

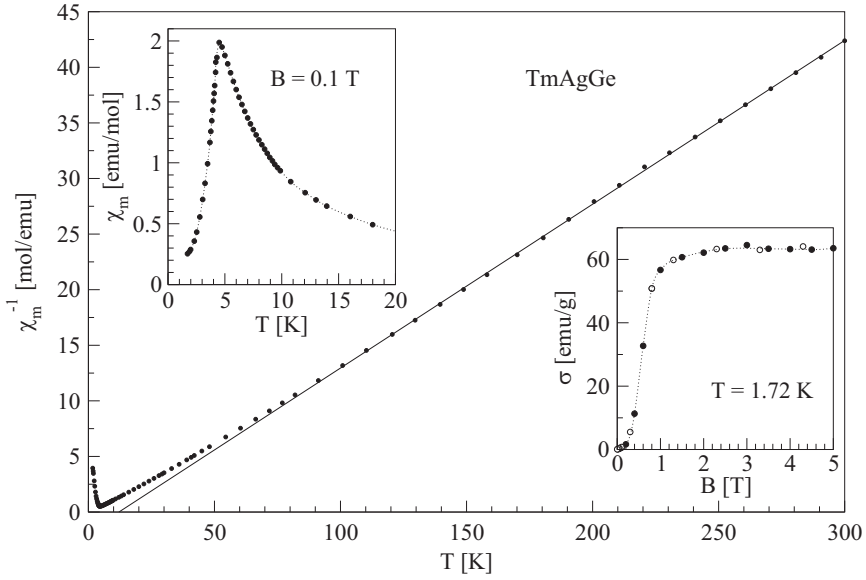

Fig. 1. Inverse magnetic susceptibility of TmAgGe. The solid line shows the Curie–Weiss fit discussed in text. The upper-left corner inset presents magnetic susceptibility at low temperatures. The bottom-right corner inset presents isothermal magnetisation curve during increasing (open symbols) and decreasing (filled symbols) of the magnetic field.

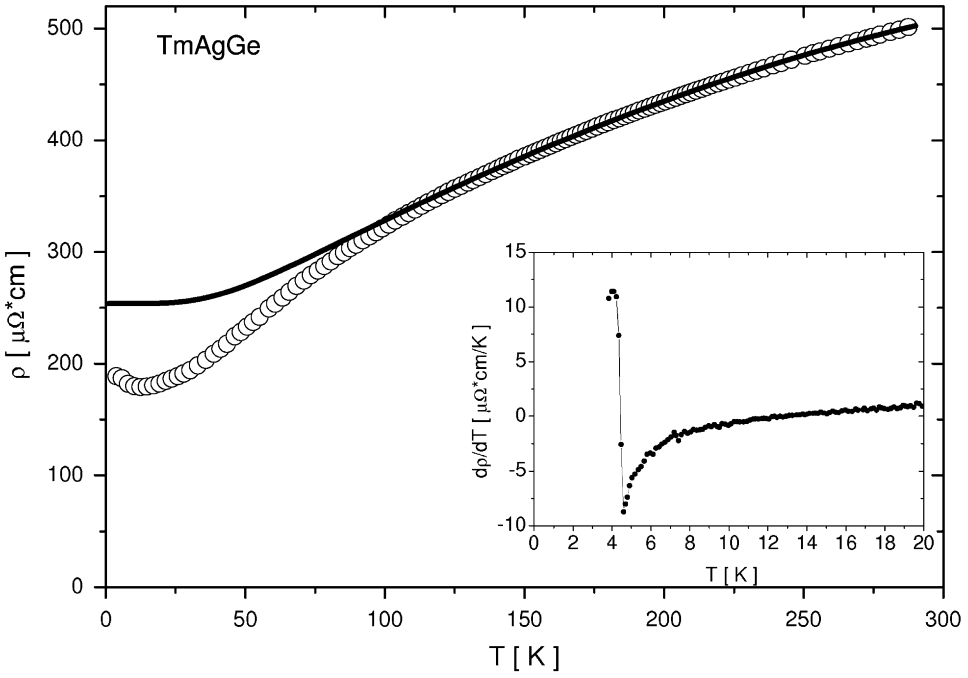

Fig. 2. Electrical resistivity of TmAgGe (open symbols). The solid line shows the fit to the Block–Grüneisen–Mott formula (see main text for details). The inset presents the low-temperature part of the derivative of electrical resistivity with respect to temperature.

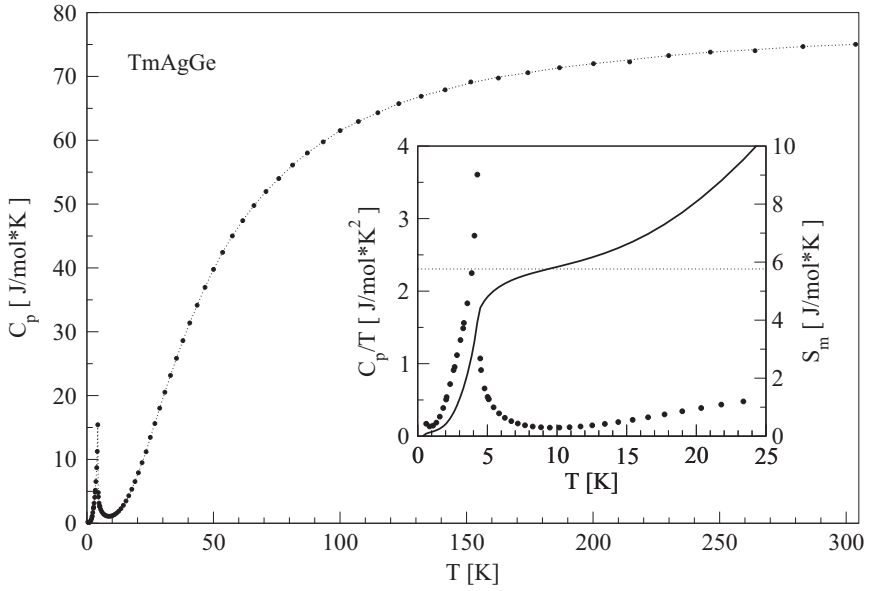

Fig. 3. Temperature dependence of the specific heat of TmAgGe. The inset presents the low-temperature part of c_p/T (dots) and magnetic entropy S_m (solid line). The entropy level $R\ln 2$ is marked by dotted line.

be close to that estimated from the specific heat data for the isostructural LuAgGe ($\Theta_D \approx 231$ K) [4]. Gradual depopulation of the crystal field levels with decreasing temperature manifests itself in the reduction of the measured resistivity below 125 K with respect to that calculated assuming constant value of the magnetic contribution in the paramagnetic region (cf. Fig. 2).

3.4. Specific heat

The temperature variation of the specific heat of TmAgGe is presented in Fig. 3. At the temperature of about 4.2 K a sharp lambda-shaped anomaly is seen, which should be related to the antiferromagnetic ordering.

The jump in the specific heat ΔC_p at T_N equals approximately 14 J/mol K which is smaller than the theoretical value 20.54 J/mol K given by the relation $\Delta C(T_N) = 2.5R((2J+1)^2 - 1)/\ ((2J+1)^2 + 1)$ with $J = 6$ appropriate for Tm^{3+} ions.

The magnetic entropy $S_m(T)$, derived from the C_p/T dependence, has a break in slope close to the transition temperature T_N with entropy reaching a value of $R\ln 2$ at the point of break. Such a value indicates ground state being a doublet or two closely separated singlets. In the unit cell of TmAgGe, the Tm^{3+} ions are located at the crystallographic position 3g with the orthorhombic

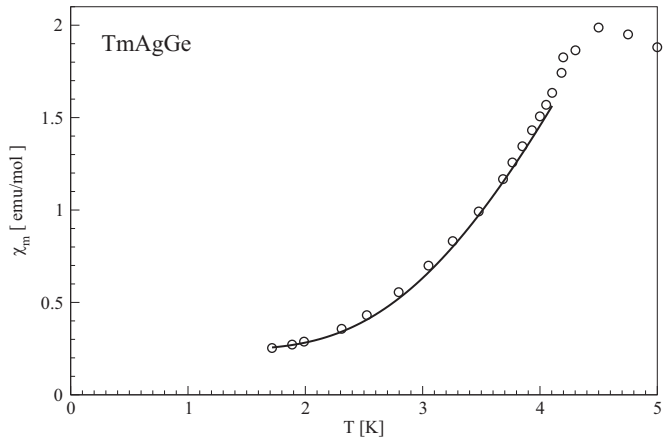

Fig. 4. The fit of the formula given by Eq. (2) to the experimental data of TmAgGe magnetic susceptibility.

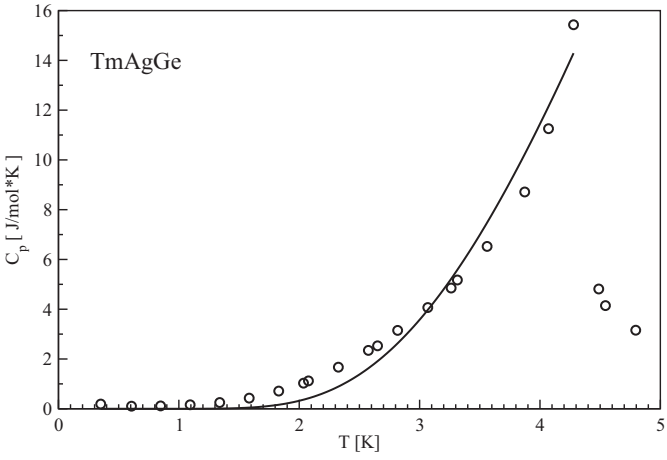

Fig. 5. The fit of the formula given by Eq. (3) to the experimental data of TmAgGe specific heat.

symmetry C_{2v} (mm^2). In the crystal field potential of this symmetry the thulium $^3H_6$ ground multiplet splits into several energy levels, with 13 singlets being the terminal case with total lifting of the $2J+1=13$ degeneracy. Such a distribution of the crystal field levels was found for isostructural TmNiAl [10]. Inelastic neutron diffraction experiment is necessary to conclude on the crystal field splitting scheme in TmAgGe.

3.5. Low temperature thermodynamic properties—AF magnons evidence

The spin-wave theory of antiferromagnetic magnons (AFM) with linear dispersion relation $\varepsilon^2(k)=\Delta^2+Dk^2$, where Δ denotes an energy gap, predicts the following temperature dependence of the magnetic susceptibility [11]

$$\chi=\tfrac{1}{3}(\chi_{\parallel}+2\chi_{\perp})=A+B\sqrt{\Delta T}e^{-\Delta/T}(\Delta-T) \quad (2)$$

where A and B are constants. It is worth to note that the parameter A is proportional to $1/\beta$, where β is an anisotropy constant.

Fitting Eq. (2) to the experimental data of TmAgGe below 4 K (see Fig. 4) gives the following parameters: $A=0.244(8)$ emu/mol, $B=0.491(11)$ emu/mol 0.16emK^2 and $\Delta=13.2(3)$ K.

In turn, the formula predicted by the spin-wave theory for the temperature variation of the specific heat in the ordered region is given by expression

$$C_{Tran}=CT^{-1/2}e^{-\Delta/T} \quad (3)$$

where C is a constant [11].

Fitting Eq. (3) to the low-temperature specific heat data of TmAgGe (see Fig. 5) yields the parameters: $C=1.15(29)\times 10^3$ JK$^{1/2}$/mol and $\Delta=15.7(9)$ K. Although the latter fit is of worse quality than that to the magnetic susceptibility data, the two obtained values of the energy gap Δ are in reasonable agreement. One may thus conclude that both the magnetic and thermodynamic characteristics of TmAgGe fulfil the predictions of the spin-wave theory for antiferromagnets. Similar description of the magnetic susceptibility and the specific was previously proposed for the isostructural compound TbAuIn [12]. However, in that latter case the energy gap Δ obtained from the analysis was as large as 58.3 K.

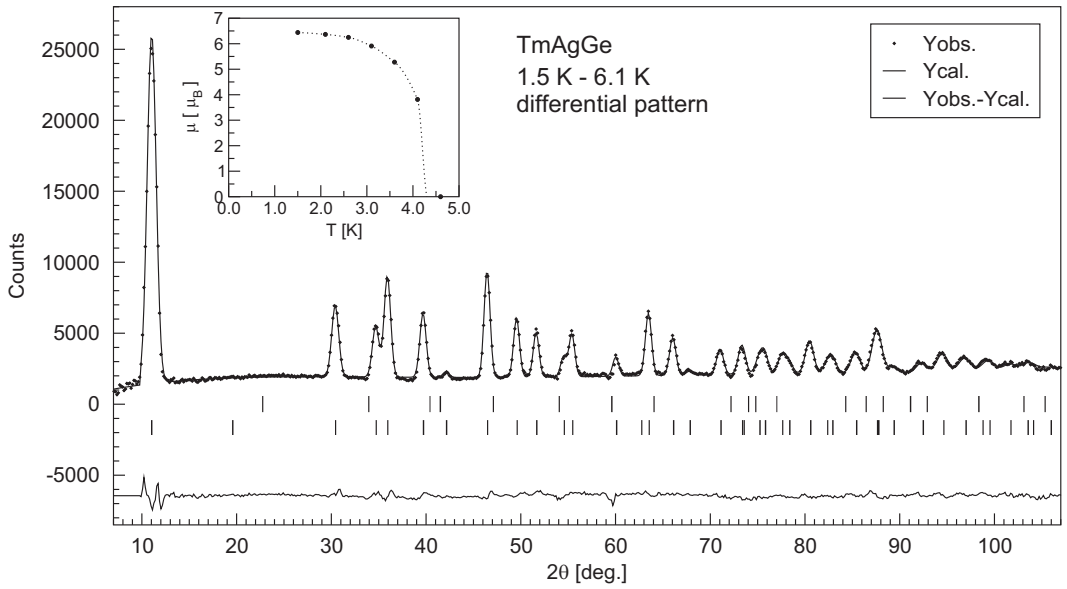

Fig. 6. Differential neutron diffraction pattern of TmAgGe together with Rietveld fit and difference plot. The pattern was made as a difference between patterns collected at 1.5 and 6.1 K. The upper row of vertical ticks indicates the positions of nuclear reflections (it is plotted just as a reference because nuclear reflections are absent in differential pattern). The next row indicates the positions of reflections originating from antiferromagnetic order.

3.6. Magnetic structure

The neutron diffraction patterns of TmAgGe taken below the Néel temperature clearly reveal the presence of some additional reflections due to the magnetic ordering. The magnetic contribution can be easily extracted by making differential pattern, like the one shown in Fig. 6. All the Bragg reflections of magnetic origin can be indexed using the propagation vector $\vec{k} = [\frac{1}{2}, 0, 0]$. In order to reduce theoretically infinite number of possible magnetic moment arrangements a group theory analysis was performed. The magnetic structures allowed by symmetry were calculated with the use of computer program *MODY* [13].

In case of the space group $G = P\bar{6}2m$ and the propagation vector $\vec{k} = [\frac{1}{2}, 0, 0]$ symmetry allows two other equivalent propagation vectors: $\vec{k}' = [-\frac{1}{2}, \frac{1}{2}, 0]$ and $\vec{k}'' = [0, \frac{1}{2}, 0]$. It means that each of the three rare earth magnetic moments present in the unit cell, i.e. Tm_1 at $x_{Tm}, 0, \frac{1}{2}$, Tm_2 at $1 - x_{Tm}, 1 - x_{Tm}, \frac{1}{2}$ and Tm_3 at $0, x_{Tm}, \frac{1}{2}$, where $x_{Tm} = 0.576(2)$ (see Table 1), may propagate with different vectors. The magnetic moments of each allowed by symmetry magnetic structure have to be parallel to basic vectors (BV) of irreducible representations (IR). The basic vectors calculated for the propagation vectors $\vec{k}$, $\vec{k}'$ and $\vec{k}''$ are listed in Table 2. For each propagation vector the atoms are divided into so-called *orbits*. Within one orbit the magnetic moments have to be of the same magnitude while the magnitude of the moments in the other orbit is independent (from symmetry point of view).

The magnetic structures constructed on the basis of the data shown in Table 2 were compared with the experimental neutron diffraction pattern. It was found that taking into account only one propagation vector one obtains non-physical results (in the magnetic structure model that accounted well for the experimental data the moment in the 2nd orbit was about 11 μ_B while the moments in the 1st were of zero magnitude). Similarly, non-physical results were obtained while two different propagation vectors were considered. The only magnetic structure that fits well the experimental data and provides reasonable values of the magnetic moments has to be constructed with the use of three different propagations vectors. Particularly, Tm_1 magnetic moment propagates with $\vec{k}'' = [0, \frac{1}{2}, 0]$, Tm_2 with $\vec{k}' = [-\frac{1}{2}, \frac{1}{2}, 0]$ and Tm_3 with $\vec{k} = [\frac{1}{2}, 0, 0]$. All the magnetic moments are confined to the basal plane. The magnetic moments directions refer to the basic vectors of τ_1 (or τ_1') in case of each propagation vector. The resulting magnetic structure, presented in Fig. 7, is a typical "triangular" magnetic structure often found in magnetically frustrated compounds. At 1.5 K the Tm magnetic moments are equal to 6.44(10) μ_B. The temperature dependence of this moment is shown in the inset to Fig. 6. The refined magnetic structure parameters are summarized in Table 3.

The derived magnetic structure of TmAgGe is in line with the results of the bulk magnetic studies on single crystals [5,6]. The latter showed a periodicity of 60° while rotating along the *c*-axis. That finding led to the conclusion that magnetic moments are aligned along the [1 1 0] direction and its equivalents, i.e. [1 0 0] and [0 1 0].

The magnetic moment of 6.44(10) μ_B at 1.5 K found from neutron diffraction is slightly smaller then the free Tm^{3+} ion which equals 7.0 μ_B, however, it is still much larger than the values found from magnetization measurements: 3.9 μ_B at $B = 5$ T and $T = 1.72$ K for polycrystalline sample (see *Magnetic behavior* section) and 4.92 μ_B at $B = 7$ T and $T = 2$ K (single-crystal with magnetic field applied along [1 1 0] direction [5,6]). The magnetic structure presented in Fig. 7 was derived from neutron diffraction data collected in the absence of external magnetic field. Applying an external magnetic field causes probably transition to a canted ferromagnetic structure as presented in Fig. 8. In such a structure the average Tm magnetic moment is given by formula $\langle\mu\rangle = (\mu/3)(1 + 2\cos 60^\circ)$. Substituting $\mu = 6.44\ \mu_B$ gives $\langle\mu\rangle$ equal to 4.29 μ_B which is in reasonable agreement with the single crystal magnetometric data. The value found for polycrystalline sample is smaller which might be caused by some preferential ordering of crystallites.

Table 2
Basic vectors (BV) of the irreducible representations (IR).

PV	$\vec{k} = [\frac{1}{2}, 0, 0]$		
IR	1st orbit		2nd orbit
	Tm_1	Tm_2	Tm_3
τ_1	[1,0,0]	[1,1,0]	[0,1,0]
τ_1'	[0,1,0]	[0,−1,0]	[0,1,0]
τ_2	[0,0,1]	[0,0,1]	–
τ_3	[1,0,0]	[−1,−1,0]	[2,1,0]
τ_3'	[0,1,0]	[0,1,0]	[2,1,0]
τ_4	[0,0,1]	[0,0,−1]	[0,0,1]
PV	$\vec{k}' = [-\frac{1}{2}, \frac{1}{2}, 0]$		
IR	1st orbit		2nd orbit
	Tm_1	Tm_3	Tm_2
τ_1	[1,0,0]	[0,1,0]	[1,1,0]
τ_1'	[1,1,0]	[1,1,0]	[1,1,0]
τ_2	[0,0,1]	[0,0,−1]	–
τ_3	[1,0,0]	[0,−1,0]	[1,−1,0]
τ_3'	[1,1,0]	[−1,−1,0]	[0,−1,0]
τ_4	[0,0,1]	[0,0,1]	[0,0,1]
PV	$\vec{k}'' = [0, \frac{1}{2}, 0]$		
IR	1 st orbit		2nd orbit
	Tm_2	Tm_3	Tm_1
τ_1	[1,1,0]	[0,1,0]	[1,0,0]
τ_1'	[1,0,0]	[−1,0,0]	[1,0,0]
τ_2	[0,0,1]	[0,0,1]	–
τ_3	[1,1,0]	[0,−1,0]	[1,2,0]
τ_3'	[1,0,0]	[1,0,0]	
τ_4	[0,0,1]	[0,0,−1]	[0,0,1]

Abbreviation PV denotes propagation vector.

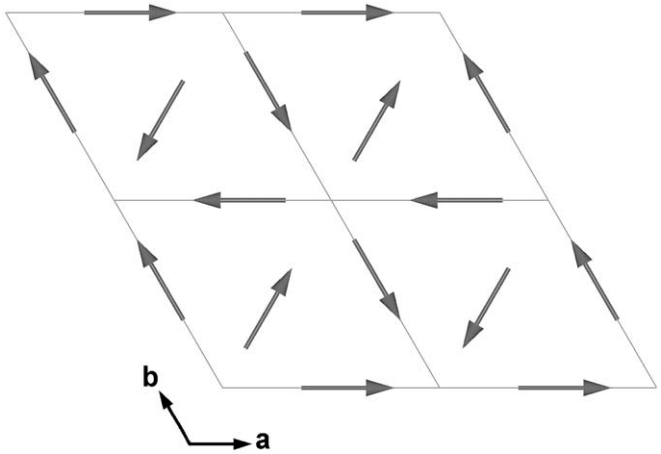

Fig. 7. The antiferromagnetic magnetic structure of TmAgGe derived from neutron diffraction.

Table 3
Refined parameters of TmAgGe magnetic structure together with residuals for profile and integrated magnetic intensities.

Atom	Tm_1	Tm_2	Tm_3
PV	$\vec{k}'' = [0, \frac{1}{2}, 0]$	$\vec{k}' = [-\frac{1}{2}, \frac{1}{2}, 0]$	$\vec{k} = [\frac{1}{2}, 0, 0]$
DMM	[1 0 0]	[1 1 0]	[0 1 0]
μ [μ_B]	6.44(10)		
χ^2		7.73	
$R_{profile}$ (%)		3.78	
$R_{magnetic}$ (%)		4.82	

The parameters were derived from the differential neutron diffraction pattern made as difference between patterns collected at 1.5 and 6.1 K. PV denotes propagation vector while DMM direction of magnetic moment.

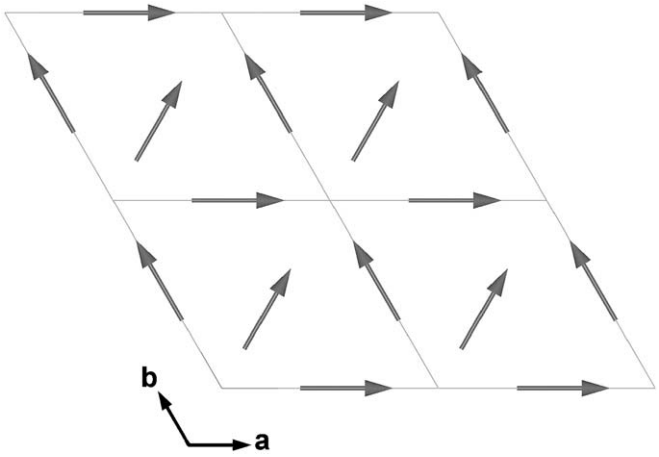

Fig. 8. The canted ferromagnetic structure of TmAgGe in the presence of external magnetic field (see discussion at the end of *Magnetic structure* subsection).

4. Summary

The ternary compound TmAgGe crystallizes in the hexagonal ZrNiAl-type crystal structure. It exhibits an antiferromagnetic ordering below 4.2 K, as derived from the magnetic susceptibility, the electrical resistivity and the specific heat data. The value of Néel temperature is in good agreement with the previously reported result. The neutron diffraction data indicate that this compound exhibits a magnetic structure with "triangular" arrangement of the Tm magnetic moments confined within the basal plane. Three different propagation vectors: $\vec{k} = [\frac{1}{2}, 0, 0]$, $\vec{k}' = [-\frac{1}{2}, \frac{1}{2}, 0]$ and $\vec{k}'' = [0, \frac{1}{2}, 0]$ are necessary to describe the magnetic order. This result follows the group theory predictions and is in good agreement with the single-crystal magnetization data. The low-temperature dependencies of the magnetic susceptibility and the specific heat reveal the presence of antiferromagnetic magnons. The value of magnetic moment derived from the neutron diffraction data is smaller than the free Tm^{3+} ion value, but well accounts for the value of the average magnetic moment in canted ferromagnetic structure, expected to form in TmAgGe in the presence of strong external magnetic field.

Acknowledgements

This research project has been supported by the European Commission under the Sixth Framework Programme through the Key Action: Strengthening the European Research Area, Research Infrastructures. Contract no: RII3-CT-2003-505925 (NMI3) and by the National Scientific Network "Strongly correlated materials: preparation, fundamental research and applications".

References

[1] G. Zanicchi, D. Mazzone, V. Contardi, R. Marazza, G. Rambaldi, D. Rossi, Gazz. Chim. Ital. 113 (1983) 257–259.
[2] G. Gibson, R. Pöttgen, R.K. Kremer, A. Simon, K.R.A. Ziebeck, J. Alloys Compd. 239 (1996) 34–40.
[3] S. Baran, M. Hofmann, J. Leciejewicz, B. Penc, M. Ślaski, A. Szytuła, J. Alloys Compd. 281 (1998) 92–98.
[4] B.J. Gibson, Investigation of the physical properties of the ternary intermetallic compounds, RETGe (RE = Sc, Y, La–Lu : T = Ag, Au), Doctoral Thesis, Loughborough University, UK, 1998.
[5] E. Morosan, S.L. Bud'ko, P.C. Canfield, M.S. Torikachvili, A.H. Lacerda, J. Magn. Magn. Mater. 277 (2004) 298–321.
[6] E. Morosan, S.L. Bud'ko, P.C. Canfield, Phys. Rev. B 71 (2005) 014445.
[7] G.D. Samolyuk, S.L. Bud'ko, E. Morosan, V.P. Antropov, P.C. Canfield, J. Phys. Condens. Matter 18 (2006) 1473–1482.
[8] J. Rodríguez-Carvajal, Physica B 192 (1993) 55–69.
[9] M. Giovannini, H. Michor, E. Bauer, G. Hilscher, P. Rogl, R. Ferro, J. Alloys Compd. 280 (1998) 26–38.
[10] N.C. Tuan, V. Sechovský, M. Diviš, P. Svoboda, H. Nakotte, F.R. de Boer, N.H. Kim-Ngan, J. Appl. Phys. 73 (1993) 5677–5679.
[11] A.I. Akhiezer, V.G. Baryakhtar, M.I. Kazanov, Usp. Fiz. Nauk 71 (1960) 533.
[12] Ł. Gondek, A. Szytuła, M. Bałanda, W. Warkocki, A. Szewczyk, M. Gutowska, Solid State Commun. 136 (2005) 26–31.
[13] W. Sikora, F. Białas, L. Pytlik, J. Appl. Crystallogr. 37 (2004) 1015–1019.